Microvascular Research 63, 139–148 (2002)
doi:10.1006/mvre.2001.2373, available online at http://www.idealibrary.com on IDEAL®

BRIEF COMMUNICATION

Automatic Tracking of Rolling Leukocytes *in Vivo*

Scott T. Acton,* Klaus Wethmar,† and Klaus Ley†

*Department of Electrical and Computer Engineering, University of Virginia, Charlottesville, Virginia 22904; and
†Department of Biomedical Engineering and Cardiovascular Research Center, University of Virginia
School of Medicine, Charlottesville, Virginia 22908

Received May 10, 2001; published online December 6, 2001

The analysis of instantaneous and average rolling leukocyte velocity is crucial to the study of inflammatory disease. In order to record features associated with leukocyte rolling, the leukocyte position must be tracked, typically by manual observation. Automated tracking of leukocytes is possible for *in vitro* studies, but not for recordings resulting from intravital experiments. Therefore, we have designed and implemented an image processing system for automated tracking of rolling leukocytes *in vivo*. The novel image processing techniques used in the tracking system successfully address the four major problems associated with tracking cells *in vivo:* background movement, severe image noise and clutter, cell deformation and contrast change, and occlusion of the target cell by other structures. We have tested the system in two experimental protocols in which leukocyte rolling is observed in venules of the mouse cremaster muscle with and without TNF-α treatment. The automated tracking system was validated by comparing automatically generated displacement and velocity data with data from the same recordings collected manually. The root mean squared error between the computed displacements and the manually measured displacements was less than 12% of the average displacement in TNF-α-treated venules. The average velocity error was also less than 12%. For untreated venules, the computed and measured displacements and velocities had an RMSE of less than 8%. The automated tracking system allows one, for the first time, to reliably track rolling leukocytes *in vivo*, thus eliminating possible investigator bias and increasing throughput.

Key Words: leukocyte rolling; video microscopy; cell tracking; image processing.

INTRODUCTION

In order to understand the mechanisms of inflammatory disease, the molecular mechanisms of leukocyte rolling, arrest and adhesion must be studied. The velocity of rolling leukocytes is an excellent predictor of the magnitude of the inflammatory response (Jung *et al.,* 1998). Currently, leukocyte rolling velocities are determined using frame-by-frame video analysis, measuring the displacement and elapsed time (Jung *et al.,* 1998; Forlow *et al.,* 2000; Kunkel *et al.,* 2000). This method of manual data collection is extremely time-consuming and introduces possible investigator bias. Automated tracking and velocity computation, if available, would significantly enhance the ability of the investigator to study leukocyte rolling, improve data collection efficiency (allowing thousands of cells to be observed), and remove operator bias.

Automated cell tracking has been applied success-

0026-2862/01 $35.00

fully to track migrating cells *in vitro* (Lackie *et al.*, 1987). The current methods of tracking include *centroid trackers* (Ghosh and Webb, 1994) and *correlation trackers* (Schütz *et al.*, 1997; Guilford and Gore, 1995; Kusumi *et al.*, 1993; Anderson *et al.*, 1992; Gelles *et al.*, 1988). Centroid trackers use the intensity "center of mass" of an object to track the position. The centroid is a reliable feature in the absence of noise, occlusion, background movement, and clutter. Correlation trackers use the correlation of a fixed template with the image to find instances of the target cell (or other particle of interest). Correlation methods are insufficient for tracking deformable targets and are also susceptible to false acquisitions in the presence of noise and clutter. In the literature, two approaches to correlation tracking are documented: correlation with a fixed intensity template of the target object (Guilford and Gore, 1995; Kusumi *et al.*, 1993; Gelles *et al.*, 1988) and correlation with a Gaussian profile (Schütz *et al.*, 1997; Anderson *et al.*, 1992). A more recent system developed by Ed Marcus Laboratories (Johnson, 2001) has been utilized for *in vitro* cell tracking (Lim *et al.*, 1998). However, the centroid and correlation trackers used for flow chamber tracking lack the robustness needed for intravital experiments.

The major roadblocks associated with intravital tracking are background movement, severe image noise and clutter, cell deformation and contrast change, and occlusion of the target cell by other structures. The goal of the present study was to develop image processing methods that solve these problems. The approach used here in the automated tracker is based on edge registration, morphological filtering (Acton and Bovik, 1998), adaptive templates, and the Kalman filter (Bar-Shalom and Li, 1993).

Major challenges in tracking cells *in vivo* include movement and clutter involved with the imaging background. For example, in mouse cremaster studies, the background moves (and becomes defocused) with each respiration (nearly twice per second). The most obvious problem is that, given other rolling leukocytes near the leukocyte of interest, the tracker may jump from cell to cell, losing track of the cell of interest. A second problem is that assumption of movement in a particular direction is no longer valid, increasing the possibility of losing track of the target cell. The third problem involved with background movement is the false computation of the cell motion statistics, because the background is not stable and the position information does not lead to reliable computation of features such as rolling velocity.

METHODS AND MATERIALS

Background Registration and Removal

The goal of the automated tracking system is to record the cell position (here, the cell centroid) until the cell leaves the field of view or until a user-specified number of frames is reached. The current tracking system relies upon manual identification of the target cells by the operator. Once the cells are selected (by "point and click"), the tracking process and data collection process are automatic. The automated tracker first performs *registration* and then *background removal*. We have designed and implemented an edge-based automated registration technique. The registration method fixes the position of background features over time. By using edges (intensity transitions), we minimize the registration error due to subtle variations in intensity. In preliminary experiments, intensity-based registration techniques proved unsuccessful in intravital microscopy due to the lack of reliable intensity patterns and the shifts in intensity over time.

The Laplacian-of-a-Gaussian (LoG) edge detector is a linear operator that combines Gaussian filtering (to reduce the response to noise and detail) with Laplacian filtering to determine the position of inflection points in intensity transitions (Marr and Hildreth, 1980). If $\mathbf{I}$ is the input image frame (one frame from the video sequence), edges can be found by locating zero crossings of the processed image $\mathbf{J}$:

$$\mathbf{J} = \Delta(\mathbf{G}_\sigma * \mathbf{I}), \tag{1}$$

where $\mathbf{G}_\sigma$ is a Gaussian filter with standard deviation σ, Δ is the Laplacian operator, and $*$ denotes convolution. The LoG paradigm uses a Gaussian scale space (Acton, 2000) to define multiscale edge detection. From the Gaussian-convolved images, one may detect edges by applying the Laplacian operator and then

finding zero crossings of the resultant signal. So, the edges are defined by **Z**:

$$Z(x, y) = |\nabla I(x, y)| \quad \text{where } J(x, y) = 0, \qquad (2)$$

and $Z(x, y) = 0$ otherwise, where $J(x, y)$ is the value of **J** at position (x, y) and $|\nabla I(x, y)|$ is the gradient magnitude of the image at position (x, y). We use the LoG zero crossings given by **Z** to locate venule boundaries (walls) for registration.

Once edges (e.g., venule boundaries) are detected, we can register the background to a fixed position by maximizing the correlation of the edge template for the current frame, $\mathbf{Z}_c$, with the edge template for the initial frame in the video sequence, $\mathbf{Z}_i$. The translation needed to register the current frame to the initial frame is the displacement (a, b) that maximizes the normalized cross correlation between $\mathbf{Z}_c$ and $\mathbf{Z}_i$.

$$c(a, b) = \frac{\sum_x \sum_y Z_c(x - a, y - b) Z_i(x, y)}{\sqrt{[\sum_x \sum_y Z_c^2(x - a, y - b)][\sum_x \sum_y Z_i^2(x, y)]}} \qquad (3)$$

The normalized cross correlation, in (3), has a range of 0 to 1, inclusive, where $c(a, b) = 1$ represents a perfect match. Typically, subimages containing only the venule of interest are used in the normalized cross correlation computation.

After registration, we time-average the registered video frames to obtain an estimate of the background and proceed to subtract the background from the video frames, leaving only the moving objects in the foreground. With this approach, the tracking operation is robust, since the tracker will not lock onto stationary background features. As an example, the time-averaged background from a mouse cremaster venule is shown in Fig. 1A, from which the features of interest, rolling leukocytes (Fig. 1C), are extracted by subtracting each individual registered video frame (Fig. 1B) from the averaged image.

Another problem associated with background movement is image blur. Although sophisticated image restoration algorithms exist (Acton and Bovik, 1999), these algorithms are not practicable for video processing, as each frame restoration requires several minutes of processing. In the current version of tracking system, image restoration is not incorporated. Instead, the tracker depends on the prediction given by the Kalman filter (discussed below) to relocate a rolling leukocyte after a blurred video frame is encountered.

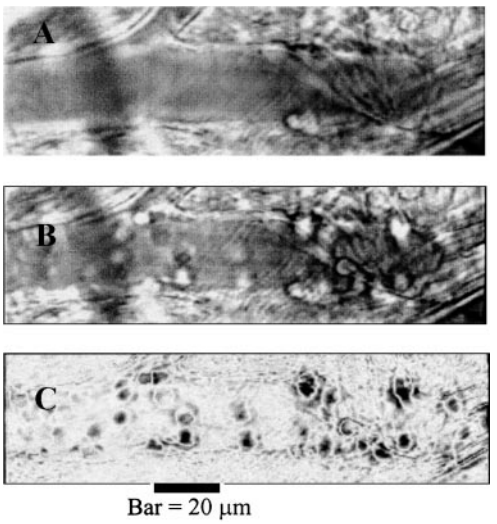

FIG. 1. An example of registration and background removal. (A) Background image averaged from registered video sequence. (B) An example image in the video sequence showing rolling leukocytes and stationary structures. (C) The image from (B) after background removal. (The image displayed is contrast-reversed.)

Video Enhancement

In addition to registration and background removal, further *enhancement* of the video is necessary to increase the robustness of the tracking procedure. The basic goal is to remove objects from the video (noise and irrelevant detail) that do not exist at the scale of interest (at the scale of the leukocytes). Within our automated tracking system, we have implemented a nonlinear method for video enhancement to be used in conjunction with the other cell tracking techniques. The method is based on shape-preserving *morphological filters* (Acton and Bovik, 1998).

The morphological operations are highly dependent upon the size and shape of the structuring element (the filter window that is set to the same shape as the leukocyte), **B**. Given a structuring element **B**, $\mathbf{I} \ominus \mathbf{B}$ is called the *erosion* of the image **I** by **B**. The erosion operation can be viewed as finding the minimal pixel intensities within the windowed sets. Therefore, the

output of $\mathbf{I} \ominus \mathbf{B}$ consists of the local minima in intensity for **I**, where locality is determined by the size of **B**. Qualitatively, erosion increases the size of dark objects and eliminates small bright objects (where "small" objects are smaller than the structuring element **B**). Conversely, the expression $\mathbf{I} \oplus \mathbf{B}$ denotes the *dilation* of **I** by **B**. The dilation operation consists of computing maxima of the windowed sets defined by the structuring element. Dilation increases the size of bright objects and eliminates small dark objects in a video frame. Bias-reduced operators can be defined by concatenating opposite operations. The *open* operation is defined by the dilation of the erosion and will smooth the image, preserve edge information, and reject bright features of insignificant scale. The counterpart, the *close* operation, is defined by dilation followed by erosion. When applied to an image, the close operation will again smooth noise without removing edges but will eradicate dark features of insignificant scale. Open and close filters are idempotent—successive application to the same signal reproduces the input image. In this way, morphological open and close operations are somewhat similar to linear ideal bandpass filters.

By further concatenation of operations we obtain the operator $(\mathbf{I} \circ \mathbf{B}) \bullet \mathbf{B}$, called the *open–close* filter. This filter has the capability to eliminate both bright and dark features that are smaller (can be inscribed into) than the structuring element **B**. We apply the open–close filter to remove noise and clutter that is beneath the scale of interest in the video microscopy sequences. Given a structuring element **B** with dimensions slightly smaller than the smallest leukocyte, we can isolate the leukocytes for tracking, as shown in Fig. 2. Notice the clutter-removing capability of the open–close filter in Fig. 2B. In this example, since the cells were approximately 20 pixels wide (at 2.4 pixels/μm), we used a circular structuring element **B** with diameter of 9 pixels (less than half the width of a typical cell).

Adaptive Template Matching for Cell Tracking

Tracking systems attempt to locate objects by comparing image data to known target models. For example, template matching methods compare the sensed imagery to stored target templates. If the target model adequately and uniquely describes the object, then the tracking algorithm can utilize the same template for successive images. However, if the cell shape or intensity changes in time, an *adaptive template* mechanism must be introduced. In tracking leukocytes, an adaptive template is required because of the changes in shape, size, and contrast due to imaging conditions and actual cellular changes. Rolling leukocytes have viscoelastic behavior (Damiano *et al.*, 1996) that is poorly matched with fixed templates. Thus, deformable templates are required for reliable tracking of rolling leukocytes *in vivo*.

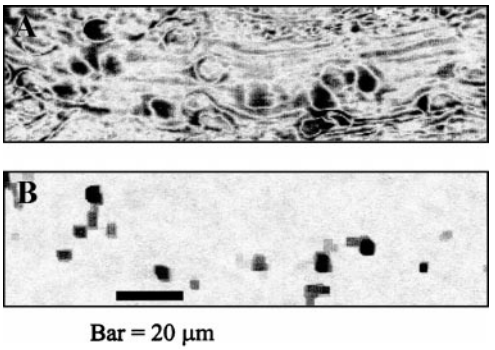

FIG. 2. An example of image enhancement using the morphological open–close filter. (A) An example image after background subtraction. (B) Enhanced image after open–close operation. Although the image in (2A) has undergone background subtraction, the rolling leukocytes have not been extracted effectively. The open–close filter result (B) allows straightforward identification and tracking of the constituent rolling leukocytes.

A method for generating an adaptive template is frame averaging. In this technique, future target profiles are estimated by a weighted average of previous target observations (Montera *et al.*, 1998). Given a template $\mathbf{T}_k$ and an observed subimage $\mathbf{O}_k$, we can form a new template by allowing

$$\mathbf{T}_{k+1} = \gamma \mathbf{T}_k + (1 - \gamma)\mathbf{O}_k, \tag{4}$$

where γ is a gain parameter ($0 < \gamma < 1$). Typically, one may employ a centroid tracker (a tracker that locates the target cell by computing the target intensity centroid) to recenter the observed target profile before averaging with the adaptive template. This adaptive procedure has the advantage of allowing the target cell to change appearance. The danger in adaptive

templates is that the tracker may acquire features that are not due to the target cell but are due to other occluding or neighboring cells. To avoid this problem, we do not update the adaptive template when the tracker is "coasting," as described below.

Cell Position Estimation and Prediction and Track Coasting

Incorporating temporal models of target motion into the tracking procedure via the Kalman filter (Bar-Shalom and Li, 1993) further improves the tracking quality given by the novel automated tracker. In the case of a brief occlusion, these temporal models may also be used to coast the track of the target, substituting the prediction for the observed track location. While the tracker is coasting, the adaptive template is not updated, avoiding corruption of the template.

We form two Kalman filters for prediction/estimation: one for the horizontal position of the leukocyte and one for the vertical position of the leukocyte (Segall *et al.*, 1999; Segall and Acton, 1998). Let i_k be the row position of a cell at video frame k. Then

$$i_{k+1} = i_k + \delta t v_k^i, \tag{5}$$

where δt is the time between frames (typically 1/30 s) and v_k^i is the velocity. The predicted row position is

$$\hat{i}_{k+1|k} = \hat{i}_{k|k} + \delta t \hat{v}_{k+1|k}^i \tag{6}$$

and the filtered row position estimate is

$$\hat{i}_{k|k} = \hat{i}_{k|k-1} + \alpha_k (i_k^0 - \hat{i}_{k|k-1}), \tag{7}$$

where α_k is a gain determined by the Kalman filter and i_k^0 is the observed position. The predicted velocity is given by

$$\hat{v}_{k+1|k}^i = \hat{v}_{k|k-1}^i + \beta_k (i_k^0 - \hat{i}_{k|k-1}) / \delta t, \tag{8}$$

where β_k is another Kalman gain. The gain α_k in (7) is increased in order to give more weight to the observations and less weight to the predictions as the track commences. The second gain β_k in (8) is decreased through time in order to give more confidence in the predicted velocity. Once we have tracked a cell for a few frames, the gains will give more weight to the predicted position and velocity. In fact, the Kalman filter provides the minimum mean squared error solution to the track position estimation and prediction problem (Bar-Shalom and Li, 1993).

Summary of the Tracking Process

Given the described image processing tools, we summarize the tracking procedure. First, a cell center is identified for tracking by the operator. Thus, the system is a point and click tracker that does not address the cell identification problem. The initial position of the cell is recomputed using the centroid of a gate around the initial selection point. From this gate, a template is extracted using the processed video that has undergone registration, enhancement, and background removal. The gate width and height are set to twice the diameter of the cell being tracked. The template is adapted according to (4) given future frames, except when the tracker is coasting. The mode of coasting is detected when the normalized cross correlation with the adaptive template falls below 0.5 (half of the potential correlation measure). The position of the highest normalized cross correlation with the adaptive template is taken as the observed cell position. Note that the adaptive template is not updated in the coast mode, and the predicted positions determined during coast mode are not recorded as observations of the cell position. Currently, we impose no limit on the number of frames that the tracker can coast. If the predicted position is found to be outside the field of view, the tracking of that particular cell is terminated. Also, the user may specify a maximum number of frames for a tracking sequence (e.g., 90 frames at 30 fps = 3 s).

Intravital Microscopy

C57BL/6 wild-type mice were obtained from the Jackson Laboratories (Bar Harbor, ME). All animal experiments were approved by the institutional animal care and use committee. In some mice, recombinant murine TNF-α (Genzyme, Cambridge, MA) was injected intrascrotally at a dose of 500 ng/mouse in a volume of 0.3 mL of sterile saline 2 h prior to the beginning of the intravital microscopic experiments as described previously (Kunkel and Ley, 1996). The cre-

TABLE 1
Experimental Results for the Rolling Leukocytes in the TNF-α-Treated Venules[a]

Cell No.	Disp. man. (μm)	Disp. auto. (μm)	Avg. vel. man. (μm/s)	Avg. vel. auto. (μm/s)	% RMSE vel.	R^2 disp.
1	29.9	32.6	10.1	11.0	9.1	0.96
2	28.4	28.7	7.8	7.9	1.0	0.95
3	15.3	15.4	5.1	5.2	1.0	1.00
4	10.6	9.7	3.6	3.3	7.9	0.96
5	16.3	15.5	4.9	4.7	4.8	1.00
6	22.4	22.7	7.5	7.6	1.3	0.99
7	10.3	10.2	3.5	3.4	1.0	0.99
8	11.0	10.2	5.6	5.2	7.7	0.99
9	13.4	13.0	4.5	4.4	3.5	1.00
10	16.2	16.2	5.4	5.4	0.0	0.99
11	11.0	9.3	3.7	3.1	15.6	0.99
12	22.4	19.9	6.8	6.0	11.3	1.00
13	14.1	13.1	4.6	4.3	6.6	1.00
14	32.2	25.3	10.8	8.5	21.3	0.98
15	19.2	19.2	6.5	6.5	0.1	1.00
16	11.1	10.3	3.8	3.5	7.2	0.99

[a] All cells were tracked for 90 frames (3 s) or until cell was not visible. Disp. refers to displacement; man. refers to manual; auto. is automatic; avg. is average; vel. is velocity; RMSE is root mean squared error.

master muscle was prepared for intravital microscopy as described (Ley *et al.*, 1995). The epididymis and testes were gently pinned to the side, exposing the cremaster microcirculation. Time 0 was set at the beginning of the cremaster muscle exteriorization. The cremaster muscle was superfused with thermocontrolled (35°) bicarbonate-buffered saline. Venules with diameters between 20 and 40 μm were observed and recorded via a CCD camera system (Dage-MTI, Inc., Model No. VE-1000CD, Michigan City, IN) on a Panasonic S-VHS recorder. The video was digitized using a Meteor II framegrabber (Matrox, Boston, MA) within a Pentium IV personal computer (Dell, Austin, TX). Tracking was implemented on a 1.5-GHz Pentium IV personal computer with 1 GB of RAM and 76 GB of storage.

RESULTS AND DISCUSSION

Tracking Rolling Leukocytes in TNF-α-Treated Venules

We analyzed 16 rolling leukocytes by recording 1440 observations of position in TNF-α-treated venules of the mouse cremaster muscle. Under these experimental conditions, leukocyte rolling is mediated by P- and E-selectin (Kunkel and Ley, 1996) with a contribution of β_2 integrins (Jung *et al.*, 1998). The automated tracker was used to compute the corresponding 1440 cell positions. Manual tracking measurements were obtained by allowing an operator to place a set of "crosshairs" over the cell center for each video microscopy frame. The frames were recorded at a spatial resolution of 320 $\times$ 240 pixels (where the pixel-to-micrometer ratio is 2.47 pixels/μm in the horizontal direction and 2.34 pixels/μm in the vertical direction) and a temporal resolution of 30 frames/s. Results for both manual and automated tracking of the leukocytes in the TNF-α-treated venules are given in Table 1.

The initial cell position for the automated tracker was obtained from the initial position recorded manually. All cells were tracked for at least 90 frames (a period of 3 s) or until the cell was not visible. Mean rolling velocity was 5.9 $\pm$ 0.4 (manual) and 5.6 $\pm$ 0.4 μm/s (automatic), consistent with earlier observations (Kunkel and Ley, 1996). The mean absolute difference between the manually recorded position and the automated tracker position averaged 1.2 μm. The devi-

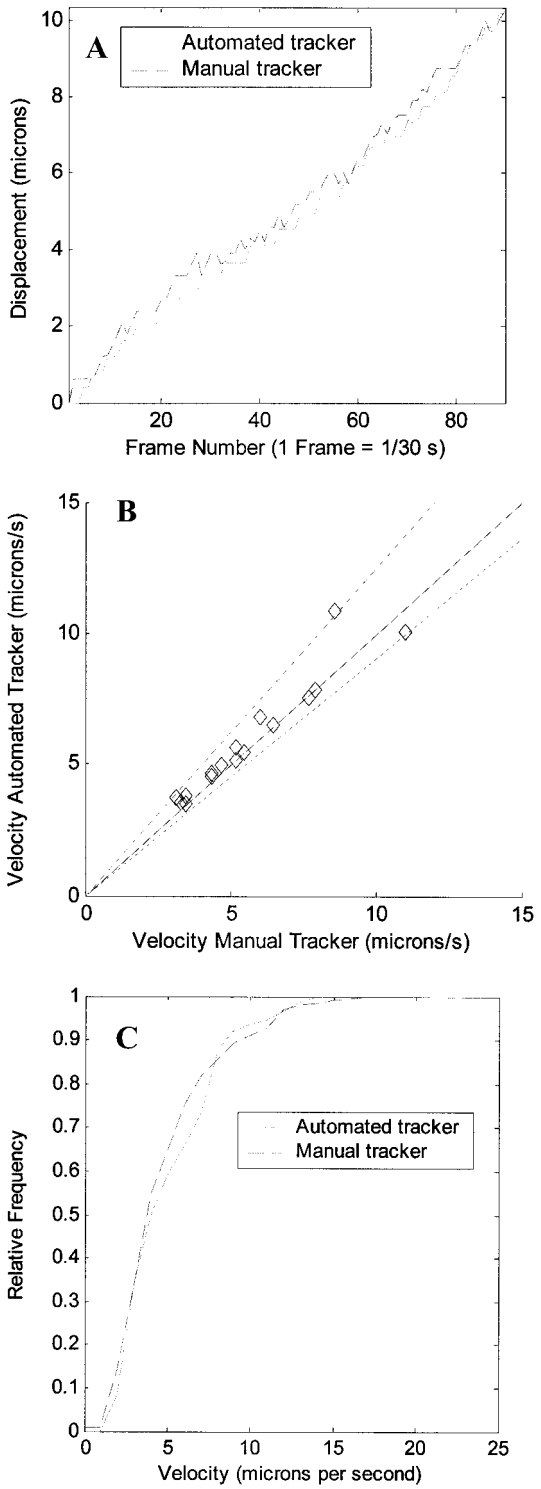

FIG. 3. Results from the experiments using TNF-α-treated venules. (A) Displacement from the origin for a single rolling leukocyte. Manually (dashed line) and automatically (solid line) computed

ation in observed average velocity from computed average velocity was 0.41 μm/s.

To compare the automated tracker to conventional tracking technology, a centroid tracker was applied to these same 16 tracking sequences. To estimate the cell position, the centroid tracker computes the intensity centroid (center of mass) in a region around the last recorded position (using the same sized region or "track gate" size as the automated tracker). The centroid tracker tested used registered video frames, but did not use the enhancement, background removal, adaptive template matching, or Kalman filter implemented with our system. Where our automated tracker had an root mean squared error (RMSE) in velocity computed of less than 12%, the centroid tracker resulted in a velocity RMSE of 66.8%. The centroid tracker only succeeds when a bright cell is superimposed on a clean, dark background. The presence of other cells, the presence of clutter such as occluding tissue, and the change in cell contrast thwart the efforts of the centroid mechanism. Although practicable for some controlled *in vitro* experiments, the centroid tracker is not a feasible solution for tracking rolling leukocytes *in vivo*.

A sample displacement result for the automated tracker is shown in Fig. 3A. The figure reveals that the automated tracker closely follows the manually recorded measurements. Note that we do not refer to the manual measurements as "ground truth," since the manual observations may be errant and are susceptible to possible investigator bias in defining the center of the cell. Cumulative histograms of instantaneous velocities are compared in Fig. 3C for the manual tracker and the automated tracker. The distributions observed manually and automatically are similar.

Assuming a linear relationship between the velocity computed from manual measurement, v_m, and the

measurements. (B) Comparison of average velocities (per cell) between the manually recorded measurements and the automated tracker results for the tracked cells. The 95% confidence interval is shown as the outermost pair of lines, and the line of identity is shown in the center of the confidence interval. (C) Cumulative histograms of manually and automatically computed instantaneous velocities.

TABLE 2
Experimental Results for the Rolling Leukocytes in the Untreated Venules[a]

Cell No.	Disp. man. (μm)	Disp. auto. (μm)	Avg. vel. man. (μm/s)	Avg. vel. auto. (μm/s)	% RMSE vel.	R^2 disp.
1	57.6	64.4	15.9	17.7	11.7	1.00
2	109.7	114.2	20.0	20.8	4.1	1.00
3	73.8	69.6	24.9	23.5	5.6	0.99
4	32.9	26.5	16.7	13.5	19.4	0.98
5	73.5	80.0	22.3	24.2	8.7	1.00
6	58.2	63.4	26.1	28.4	8.9	1.00
7	18.8	19.8	14.5	15.3	5.5	0.99
8	91.4	92.7	21.1	21.4	1.5	1.00
9	47.2	50.2	20.5	21.8	6.4	0.97
10	17.1	15.0	10.5	9.2	12.6	0.99
11	98.0	102.8	22.8	23.9	4.9	1.00
12	74.5	71.7	25.1	24.2	3.8	0.99

[a] All cells were tracked for 90 frames (3 s) or until the cell was not visible. Disp. refers to displacement; man. refers to manual; auto. is automatic; avg. is average; vel. is velocity; RMSE is root mean squared error.

velocity computed from the automated tracker, v_t, we have

$$v_m = Bv_t. \quad (9)$$

The 95% confidence interval for B in this case is $B \in [0.90, 1.0]$. The associated R^2 value is 0.91, which shows a strong correlation between manual measurements and the tracking software. Figure 3B shows a plot of average velocities, comparing manually recorded measurements to the velocities computed by the automated tracker. The figure also delineates the 95% confidence interval for the average velocities.

Tracking Rolling Leukocytes in Untreated Venules

In untreated venules, we used the automated tracker to observe P-selectin-dependent rolling (Ley *et al.*, 1995). We have analyzed 12 cells rolling in untreated venules by recording 1080 observations manually and automatically using the methods described in this paper. For detailed results, consult Table 2. The measurements recorded manually differed from the automatically computed position measurements by 4.0 μm, on average. Average rolling velocity for all cells was 20.0 $\pm$ 0.4 (manual) and 20.3 $\pm$ 0.4 μm/s (automatic), similar to the results of Jung *et al.* (1997). The difference in manually observed and automatically computed velocity was 1.45 μm/s for this experiment. The difference is greater than in the TNF experiment due to the higher velocities and the increased difficulty of tracking the quickly rolling cells. If the automated tracker loses track on a rolling leukocyte for a given frame, it is more difficult to reacquire the cell in subsequent frames if the leukocyte is rolling rapidly, due to increased uncertainty in the predicted position.

Again, we applied the conventional centroid tracker to the same 12 sequences recorded from the untreated venules. Where the automated tracker presented here gave a velocity RMSE of less than 8%, the centroid tracker led to a velocity RMSE of 87.2%. In these sequences, the centroid tracker lost track because of poor contrast, high clutter, dominant background features (the venule wall is brighter than the cells in certain situations), and lack of adaptability.

A sample plot of displacement from the automated tracker for one cell in trauma is shown in Fig. 4A for both the manual tracker and the automated tracker. Cumulative histograms of instantaneous velocities are given in Fig. 4C for manual tracking and for automated tracking. The automated tracker mimics the manually recorded measurements in the individual leukocyte paths and in the ensemble statistics.

Using the linear model described in Eq. (9), the 95% confidence interval for B is $B \in [0.90, 1.0]$. The R^2 value is 0.91, which is consistent with the results obtained from the treated venules. Examining the average velocity of the cells in trauma (average velocity =

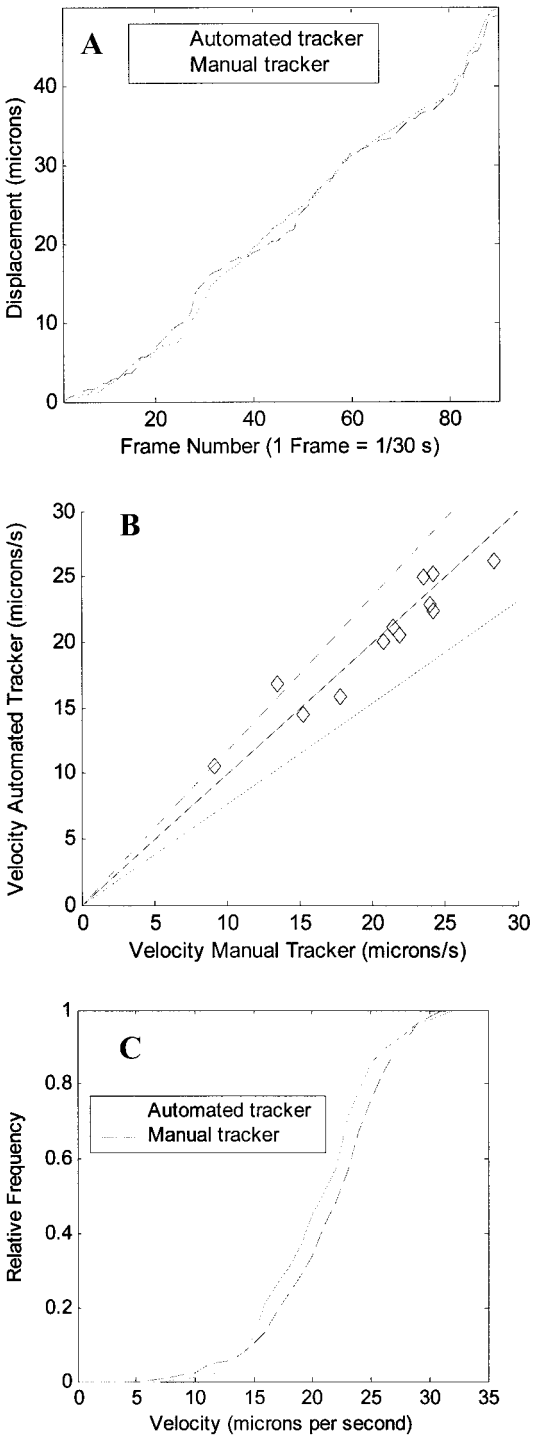

FIG. 4. Results from the experiments using untreated venules. (A) Displacement from the origin for a single rolling leukocyte. Manually (dashed line) and automatically (solid line) computed measurements. (B) Comparison of average velocities (per cell) between the manually recorded measurements and the automated tracker results for the tracked cells. The 95% confidence interval is shown as the outermost pair of lines, and the line of identity is shown in the center of the confidence interval. (C) Cumulative histograms of manually and automatically computed instantaneous velocities.

20.0 ± 0.4 μm/s), the deviation is 5.6%, less than that found for the TNF-α-treated cells (6.9%). Taking into account the overall average velocity, the tracking experiment with the cells in trauma is as successful as the automated tracking of the TNF-treated cells. A scatter plot comparing manually recorded velocities with automatically computed velocities is given in Fig. 4B, with the linear regression and 95% confidence interval superimposed. Note that the velocity measurements from the manual and automated trackers are almost identical in most cases.

Flexibility and Ease of Use

In the 28 sequences tested, the automated tracker was able to maintain track in cases of cell collisions, cessation of motion (adherence), and microjumps (instantaneous velocity changes). The two sets of experiments (untreated and treated venules) show the flexibility in terms of the range of velocities (from 3 to 30 μm/s). In future experiments, we will test the performance of the tracker in cases of severe clutter where the tissue is not as clear optically as in the cremaster studies presented here.

For ease of use, the tracker only requires the initial cell position, which is obtained by clicking on the center of the target cell. So, no additional parameters or thresholds need to set for tracking. For tracking multiple cells within the same video sequence, we have built an interface that allows the operator to inspect a digitized video and select multiple cells for automatic tracking. On a 1.5-GHz Pentium-IV-based system with 1 GB of RAM, a 90-frame sequence (3 s of video) requires 0.06 s of processing. In the case of tracking N cells for 90 frames each, the computational expense is $0.06N$ s. Hence, the processing time (excluding display of resultant video) is negligible compared to the video acquisition time.

In conclusion, we have developed and validated an automatic video tracking system for observing the

motion of rolling leukocytes *in vivo*. The automated tracker uses digitized video microscopy to locate and follow leukocytes rolling through venules under baseline (untreated) or severely inflamed (TNF-α) conditions. Innovative image processing techniques have been employed in the automated tracker to combat background movement, severe image noise and clutter, cell deformation and contrast change, and occlusion of the target cell. The image processing system has been validated for intravital microscopy in TNF-α-treated venules and in untreated venules. Using over 2500 observations of leukocyte position, we demonstrate that automated tracking of rolling leukocytes *in vivo* is feasible and that reliable automated tracking of rolling leukocytes can be achieved. The automated tracker holds promise for expansion of the number of observations recorded in intravital experiments and for removal of investigator bias.

ACKNOWLEDGMENTS

This work was in part supported by NIH R01 HL 64381 to KL. STA is supported in part by the Army Research Office under DAAD19-01-1-0594.

REFERENCES

Acton, S. T. (2000). Diffusion-based edge detectors. *In* "The Handbook of Image and Video Processing." Academic Press, New York, pp. 433–447.

Acton, S. T., and Bovik, A. C. (1999). Piecewise and local image models for regularized image restoration using cross validation. *IEEE Trans. Image Proc.* **8,** 652–665.

Acton, S. T., and Bovik, A. C. (1998). Order statistics in image processing. *In* "Handbook of Statistics Volume 17: Order Statistics and Their Applications" (N. Balakrishnan and C. R. Rao, Eds.), Elsevier, New York, pp. 603–641.

Anderson, C. M., Georgiou, G. N., Morrison, I. E. G., Stevenson, G. V. W., and Cherry, R. J. (1992). Tracking of cell surface receptors by fluorescence digital imaging microscopy using a charge-coupled device camera. *J. Cell Sci.* **101,** 415–425.

Bar-Shalom, Y., and Li, X. R. (1993). "Estimation and Tracking: Principles, Techniques, and Software." Artech House, Boston, MA.

Damiano, E. R., Westheider, J., Tözeren, A., and Ley, K. (1996). Variation in the velocity, deformation, and adhesion energy density of leukocytes rolling within venules. *Circ. Res.* **79,** 1122–1130.

Forlow, S. B., White, E. J., Barlow, S. C., Feldman, S. H., Lu, H., Bagby, G. J., Beaudet, A. L., Bullard, D. C., and Ley, K. (2000). Severe inflammatory defect and reduced viability in CD18 and E-selectin double mutant mice. *J. Clin. Invest.* **106,** 1457–1466.

Gelles, J., Schnapp, B. J., and Sheetz, M. P. (1988). Tracking kinesin-driven movements with nanometre-scale precision. *Nature* **331,** 450–453.

Ghosh, R. N., and Webb, W. W. (1994). Automated detection and tracking of individual and clustered cell surface low density lipoprotein receptor molecules. *Biophys. J.* **66,** 1301–1318.

Guilford, W. H., and Gore, R. W. (1995). The mechanics of arteriole-interstitium interaction. *Microvasc. Res.* **50,** 260–287.

Johnson, B. D. (2001). Automated imager stalks cells. *Photon. Spectra* **35,** 50.

Jung, U., Norman, K. E., Ramos, C. L., Scharffetter-Kochanek, K., Beaudet, A. L., and Ley, K. (1998). Transit time of leukocytes rolling through venules controls cytokine-induced inflammatory cell recruitment in vivo. *J. Clin. Invest.* **102,** 1526–1533.

Kunkel, E. J., Dunne, J. L., and Ley, K. (2000). Leukocyte arrest during cytokine-dependent inflammation *in vivo*. *J. Immunol.* **164,** 3301–3308.

Kunkel, E. J., and Ley, K. (1996). Distinct phenotype of E-selectin deficient mice: E-selectin is required for slow leukocyte rolling in vivo. *Circ. Res.* **79,** 1196–1204.

Kusumi, A., Sako, Y., and Yamamoto, M. (1993). Confined lateral diffusion of membrane receptors as studied by single particle tracking (nanovid microscopy). Effects of calcium-induced differentiation in cultured endothelial cells. *Biophys. J.* **65,** 2021–2040.

Lackie, J. M., Chaabane, N., and Crocket, K. V. (1987). A critique of the methods used to assess leukocyte behavior. *Biomed. Pharmacother.* **41,** 265–278.

Ley, K., Bullard, D. C., Arbones, M. L., Bosse, R., Vestweber, D., Tedder, T. F., and Beaudet, A. L. (1995). Sequential contribution of L- and P-selectin to leukocyte rolling in vivo. *J. Exp. Med.* **181,** 669–675.

Lim, Y. C., Snapp, K., Kansas, G. S., Camphausen, R., Ding, H., and Luscinskas, F. W. (1998). Important contributions of P-selectin glycoprotein ligand-1-mediated secondary capture to human monocyte adhesion to P-selectin, E-selectin, and TNF-α-activated endothelium under flow in vitro. *J. Immunol.* **161,** 2501–2508.

Marr, D., and Hildreth, E. (1980). Theory of edge detection. *Proc. R. Soc. London* **B207,** 187–217.

Montera, D. A., Rogers, S. K., Ruck, D. W., and Oxley, M. E. (1998). Object tracking through adaptive correlation. *In* "Optical Pattern Recognition IV," SPIE Vol. 1959.

Schütz, G. J., Schindler, H., and Schmidt, Th. (1997). Single-molecule microscopy on model membranes reveals anomalous diffusion. *Biophys. J.* **73,** 1073–1080.

Segall, C. A., Chen, W., and Acton, S. T. (1999). Video tracking using the morphological pyramid. *J. Electron. Imag.* **8,** 176–184.

Segall, C. A., and Acton, S. T. (1998). Multi-scale video tracking. *In* "Workshop on the Detection and Classification of Difficult Targets." Redstone Arsenal, Huntsville, AL, June 9–10.